ACS Photonics

Article

Cite This: ACS Photonics 2019, 6, 189−195

pubs.acs.org/journal/apchd5

Optical Coupling between Resonant Dielectric Nanoparticles and Dielectric Nanowires Probed by Third Harmonic Generation Microscopy

Kirill I. Okhlopkov,[†] Pavel A. Shafirin,[†] Alexander A. Ezhov,[†] Nikolay A. Orlikovsky,[‡] Maxim R. Shcherbakov,[†,¶] and Andrey A. Fedyanin*[,†]

[†]Faculty of Physics, Lomonosov Moscow State University, Moscow, Russia

[‡]Bauman Moscow State Technical University, Moscow, Russia

[¶]School of Applied and Engineering Physics, Cornell University, Ithaca, New York, United States

Supporting Information

ABSTRACT: Localized electromagnetic modes and negligible Ohmic losses dictate the growing interest to subwavelength all-dielectric nanoparticles. Although an exhaustive volume of literature dealt with interaction of all-dielectric nanostructures with free-space electromagnetic fields, they received little attention as integrated photonic elements. We present an experimental and numerical study of optical coupling between a resonant subwavelength silicon nanodisk and a silicon nanowire, as probed by third harmonic generation microscopy and full-wave simulations. First, by placing the nanodisks at different distances from the nanowire, we observed third harmonic intensity modulation by a factor of up to 4.5. This modulation is assigned to changes in the local field enhancement within the nanodisks caused by their coupling to the nanowires and subsequent shifting and broadening of their magnetic-type resonances. Interestingly, although the nanowire presents an additional loss channel for the nanodisk, we observed an increase in the local field strength within the nanodisk, as verified by rigorous full-wave simulations. Inversely, for the gap sizes that are smaller than ≈200 nm, we observe the influence of the nanoparticles on the propagation properties of the fundamental waveguide modes of the nanowire. The better understanding of the mutual influence of the Mie-resonant nanoparticles and waveguiding structures heralds integration of the former on-photonic chips.

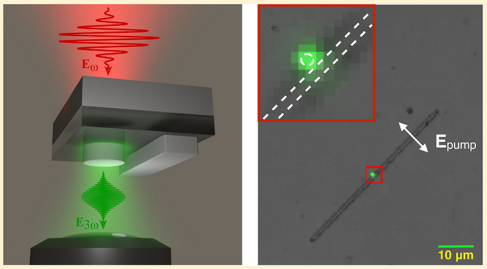

KEYWORDS: *optical coupling, dielectric nanowire, silicon nanoparticles, third harmonic generation microscopy*

Nanophotonics deals with optical properties of nanoscale materials, of which nanoparticles (NPs) play a central role, for they exhibit strong shape-dependent resonances utilized in light harvesting,[1] medicine, and biological applications.[2] While the shape of NPs in many ways determines their optical properties,[3] it is important to disclose new degrees of freedom to control their resonances. Resonances of individual NPs can be affected by changing their environment[4] or by bringing them in the near-field vicinity of other resonant systems.[5] Optical coupling between closely spaced NPs brings about hybridization of modes giving additional means to shape their spectra and local fields.[6] This property was extensively used to demonstrate the plasmonic analog of electromagnetically induced transparency,[7] designing plasmonic waveguides,[8] and so-called plasmon rulers.[9−11] However, many applications, including nanophotonic circuitry, impose severe restrictions to levels of nonradiative losses in materials, for which plasmonic NPs do not always qualify.

A new paradigm in nanophotonics has recently emerged, where metallic NPs are challenged by those made of high-index dielectrics.[12−14] Apart from studies on single-particle scattering,[15,16] optical properties of dielectric NP formations in dimers,[17,18] trimers,[19] and higher-order oligomers[20,21] have been explored, with much stress put on the fundamental mode of NPs, the magnetic dipolar (MD) mode. Low Ohmic losses of all-dielectric NPs make them also appealing for nonlinear-optical applications, where high optical powers are a necessity.[22−27] Finally, and in contrast to plasmonic NPs, all-dielectric NPs can be fabricated using CMOS-compatible materials, most importantly silicon,[28] making them perfect candidates for integrated photonics devices, including waveguides,[29,30] nanoantennas,[31] and nanolasers.[32] However, there have been very few attempts to consider silicon nanoparticles for integrated photonics elements,[33,34] and we believe further studies are necessary.

In this paper, we disclose two regimes of optical coupling between a single subwavelength silicon nanodisk and a silicon nanowire that acts as a dielectric waveguide. Subwavelength nanodisks are designed to exhibit magnetic dipolar resonances in the near-infrared, which are experimentally shown to

Received: October 5, 2018
Published: December 18, 2018

DOI: 10.1021/acsphotonics.8b01386
ACS Photonics 2019, 6, 189−195

increase the third-harmonic up-conversion efficiency by a factor of up to 25 with respect to bulk silicon. Placing the nanodisks within a subwavelength distance from the nanowires, we observed a strong modification of the local fields within the nanodisk, which results in a modulation of their nonlinear-optical response by a factor of up to 4.5. Counterintuitively, the nanowires can constructively enhance the nonlinear response of the nanodisks, which is supported by full-wave simulations of the local fields within the nanodisks. At the same time, by placing the nanodisks at the distance less than 200 nm from the nanowire, we observe the direct influence of the resonant nanodisks and waveguide modes through scattering losses of the fundamental TM and TE modes. To our knowledge, our findings present the first nonlinear-optical study of all-dielectric Mie-resonant particles interacting with silicon nanowires that can act as dielectric waveguides, opening new ways of tailoring their response, both in linear and nonlinear regimes.

RESULTS AND DISCUSSION

Sample Design and Fabrication. Among many shapes and designs for all-dielectric NPs that possess localized Mie resonances, a nanodisk is the most well-understood geometry[35] from those accessible by lithography. Silicon was chosen as a material for proposed structures for its CMOS-compatibility, high refractive index, and large value of third-order susceptibility, which plays a significant role in our experiments. The proposed "silicon nanodisk–nanowire" pairs were fabricated out of a silicon-on-insulator wafer (Figure 1a) by

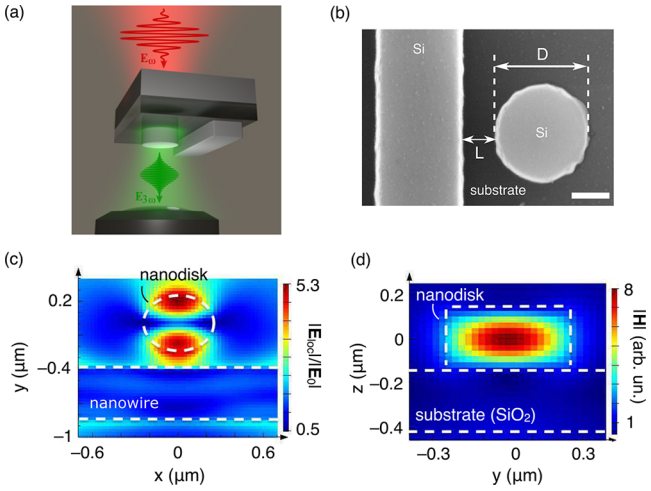

Figure 1. (a) Illustration of THG from the nanodisk coupled to the nanowire. (b) Scanning electron micrograph of the sample with D = 515 nm and L = 165 nm (top view). The scale bar is 200 nm. (c) Calculated distribution of the normalized electric field strength in the middle xy-section of the nanowire and nanodisk. (d) Calculated distribution of the normalized magnetic field magnitude in the middle yz-section of the nanodisk. Both maps are given for D = 480 nm, L = 150 nm, and an excitation wavelength of 1.53 μm. The white dashed lines indicate the boundaries of structures.

electron-beam lithography and reactive-ion etching. The thicknesses of both the top silicon and the buried SiO_2 layers were 280 nm. The thicknesses of nanowire and nanodisk were determined by atomic force microscopy, while the thickness of the buried SiO_2 layer was obtained using spectroscopic ellipsometry (see Methods). Nine combinations of silicon nanodisk diameters (D) and the gap sizes between a disk and a nanowire (L) were fabricated, as given in Table 1; here, D = 380, 430, and 480 nm, and L = 105, 185, and 320 nm. These numbers are the averaged values obtained by scanning electron microscopy. The purpose of varying the gap size is to modify the optical coupling between nanodisks and nanowires, whereas varying the nanodisk diameter gives us flexibility in tuning the spectral position of the MD mode. The resonance at a wavelength of 1.53 μm in the nanodisk is demonstrated numerically for D = 480 nm by observing a resonant enhancement of local electric (Figure 1c) and magnetic (Figure 1d) fields, which reveal an x-oriented MD-type field distribution. For smaller diameters, the central wavelength of the resonance was determined to be blue-shifted by approximately 70 and 150 nm with respect to the pump wavelength; see Supporting Information for details. For the nanowire to be suitable for a laser wavelength of 1.545 μm and to present a potential in-/out-coupling channel, its width was chosen to be 435 nm. The length of each nanowire is 50 μm. A scanning electron microscope image of a typical "nanowire–disk" pair with a gap size of 165 nm and with a nanodisk diameter of 515 nm is shown in Figure 1b.

Table 1. Third Harmonic Generation Intensity from Silicon Nanodisks Coupled to Silicon Nanowires Normalized by the THG from the Silicon Substrate[a]

	gap size L (nm)			
D (nm)	105	185	320	$\lambda_{pump} - \lambda_{MD}$ (nm)
380	0.7	0.9	0.9	150
430	1.0	2.4	1.4	70
480	3.8	17.0	6.5	10

[a]The normalized signal from the nanowire without a nearby disk is 0.8. Typical relative signal errors are ±20%. λ_{MD} is the central wavelength of the MD resonances.

Nonlinear Microscopy. When an optical system is excited at its resonant wavelength, electromagnetic fields within the system may be much higher than those in the incoming wave. Optical coupling is known to disturb resonance conditions in nanoparticles, affecting the structure of the local fields, which may be, in turn, probed by measuring the nonlinear optical response. Here, we probe optical coupling by illuminating the nanodisks with tightly focused femtosecond laser pulses and collecting scattered third harmonic signal generated by the nonlinear polarization $\mathbf{P}^{(3)}_{3\omega}(\mathbf{r}) = \varepsilon_0 \hat{\chi}^{(3)}_{Si} : \mathbf{E}_\omega(\mathbf{r})\mathbf{E}_\omega(\mathbf{r})\mathbf{E}_\omega(\mathbf{r})$ in silicon parts of the structure. We can safely neglect third harmonic generation (THG) from the buried oxide, as the cubic susceptibility of SiO_2 is 3 orders of magnitude smaller than the nonzero components of $\hat{\chi}^{(3)}_{Si}$.[36,37] In our setup, the pump pulses came from an Er-ion-doped fiber laser system with a carrier wavelength of λ = 1.545 μm, as shown in Figure 2a. The pulses produced up to 7 kW of peak power at the back of the substrate, being focused at the structures to a waist of 3 μm in diameter. The forward-emitted THG signal was collected by a scanning confocal microscope, which was capable of mapping the intensity of the THG over the confocal image of the sample that was taken simultaneously. For further measurement details, refer to Methods.

In accord with previous findings,[22] we observed that exciting the MD mode of the nanodisks significantly enhances THG. Shown in Figure 2b–d are three snapshots of a "nanowire–disk" pair, with the small red squares circumscribing the

DOI: 10.1021/acsphotonics.8b01386
ACS Photonics 2019, 6, 189–195

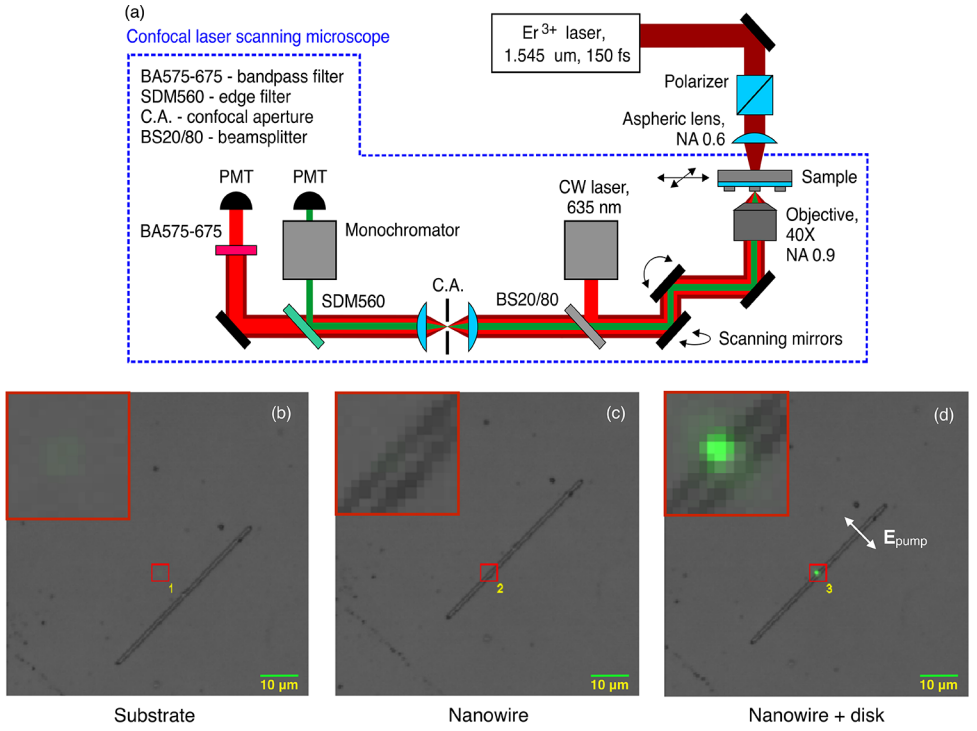

Figure 2. (a) Third harmonic generation confocal microscopy setup (see Methods for details). (b–d) Third harmonic generation maps (green) laid over confocal images of the sample (gray). Small red squares circumscribe the pump beam and represent the integration area used to measure THG signals. Three cases are shown: (b) the pump illuminates the substrate, THG is barely seen; (c) the pump illuminates the nanowire, THG is weaker than in the case (b); (d) the pump illuminates the nanowire and the disk, THG is bright. Insets are close-ups on the red squares.

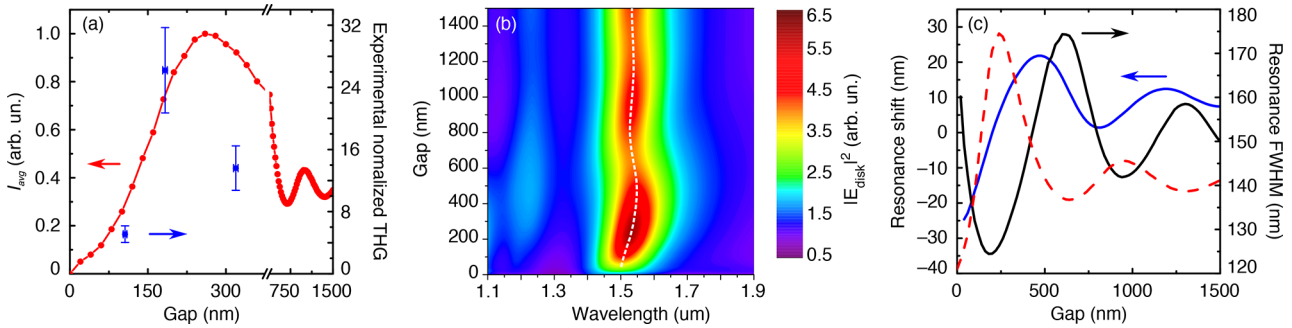

Figure 3. (a) Experimental normalized THG enhancement from resonant nanodisks (D = 480 nm) as a function of the gap between the nanodisk and the nanowire (blue squares) and normalized local electric fields, given by eq 1 (connected red circles). (b) Electric field strength distribution over the volume of the nanodisk as a function of gap L and wavelength. White dashed curve indicates the nanodisk's MD resonance position. (c) MD resonance parameters as a function of gap L, with its central position plotted in blue, and full width at half-maximum plotted in black. The dashed curve is the same as the red curve from (a), provided for comparison.

position of the pump, which was polarized perpendicularly to the nanowire. In these images, the nanodisk cannot be fully resolved due to its small size and resolved as a slight protrusion in the middle of the nanowire. The gray scale confocal images are taken under CW laser illumination, while the green color represents the emitted THG signal. As opposed to the THG signal from the Si–SiO_2 substrate in Figure 2b, and from the nanowire in Figure 2c, the nanodisk provides a bright and distinct THG spot as shown in Figure 2d. Specifically, here, the THG signal from the nanodisk is stronger than that from the silicon substrate by a factor of 17. Given that, under the same conditions, smaller nanodisks provided an order of magnitude less intense THG, we conclude that the main contribution of THG in our observations come from the nanodisks with resonantly excited MD resonances.

In order to experimentally access different regimes of optical coupling between the resonant nanodisk and the nanowire, we expand our measurement scope by considering different gap sizes between the particles L. A summary of the THG microscopy results is given in Table 1 for nine combinations of D and L; here, THG from the nanostructures was normalized by the THG measured at the substrate. First, we quantify the difference between THG measured for the resonant nanodisks (D = 480 nm) and nonresonant nanodisks (D = 430 and 380 nm), with the latter providing up to 17.0/0.7 = 24 times less THG yield, with a typical statistical error of ±20%. Note that, for the smallest disks, proper positioning of the pump beam on the nanodisks was not guaranteed, since the THG signal measured at the bare nanowire was on the same level (≈ 0.8) with the THG from the nanodisks (≈0.7–0.9). Second, a clear

DOI: 10.1021/acsphotonics.8b01386
ACS Photonics 2019, 6, 189–195

difference, by a factor of 5, is observed between the THG signals from the disks of the same diameter but different gap sizes, with a local maximum observed for a gap size of L = 185 nm. Below, we numerically address this observation and show that the presence of a nanowire can enhance field localization in the nanodisk and constructively amend its nonlinear response. We provide measurement results for the orthogonal pump polarization in Supporting Information. There, the nanowire itself demonstrates considerable, by a factor of 6, THG enhancement with respect to the substrate, which disrupts interpretation.

Numerical Calculations. A full-wave simulation of the system under study was performed using a commercially available Maxwell's equations solver, see Methods for details. In order to verify the strong dependence of the nonlinear-optical response of the nanodisk on its distance to the nanowire and separate it from any other sources of THG, we calculated and integrated the local fields within the resonant disk as a function of L. In order to mimic the third-order nonlinear response, we plot in Figure 3a the following quantity:

$$I_{\mathrm{avg}} = \int_{\mathrm{disk}} \int_{\mathrm{pulse}} |\mathbf{E}(\mathbf{r}, \nu)|^6 \mathrm{d}V \mathrm{d}\nu \tag{1}$$

where $\mathbf{E}(\mathbf{r}, \nu)$ is the calculated electric field strength distribution, which is integrated over the spectrum of laser pulse and over the volume of the nanodisk.

Although this quantity is not straightforwardly connected to the measured THG signals, it gives us important insights about how the nanowire affects the local fields within the nanodisk. The calculated dependences of I_{avg} on L for nanodisks with all experimentally available diameters (D = 480, 430, and 380 nm) can be found in the Supporting Information. The dependence of I_{avg} on L is nonmonotonic for the case of a nanodisk with a diameter of 480 nm and shows damped oscillations saturating at a level of about $I_{\mathrm{avg}}/I_{\mathrm{avg}}^{\mathrm{max}}$ = 0.4 for large L, where the nanowire is placed considerably far from the nanodisk. This means that, in agreement with our experimental observations, the nanowire can constructively amend the local fields within the nanodisk. Blue squares show the measured enhancement of the THG from the nanodisks for three values of L. Note that the plotted values differ from those in Table 1; for here, we have optimized the detection spectral range of the THG signal. To determine the influence of nanowire to the local electric fields inside the nanodisk in our simulations, we have replaced nanowire by a mirror and calculated the dependence of I_{avg} on gap L (Figure 4b). The maxima and the minima of I_{avg} are achieved at the same values of L in the cases of nanowire and mirror. It can be seen that the nanowire plays a role of reflector for nanodisk's electric fields that in turn leads to oscillations of I_{avg}. An explanation of the nonmonotonic behavior is given in Figure 3b,c. We have calculated the spectra of electric field strength distributions $|E_{\mathrm{disk}}|^2$, which is integrated over the all volume of the nanodisk, at different gaps, presented in Figure 3b. The strong local electric fields enhancement is observed for a wavelength of 1.5 μm and associated with the MD resonance excitation. To clarify the MD resonance behavior, we plotted the central wavelength and full-width at half-maximum (FWHM) of the nanodisk's MD scattering resonance as a function of L, presented in Figure 3c with blue and black curves, respectively. It is very instructive that the FWHM of the resonance is strongly modulated by the nanowire, varying from 125 nm at $L \approx$ 200 nm to 175 nm at $L \approx$ 600 nm. By

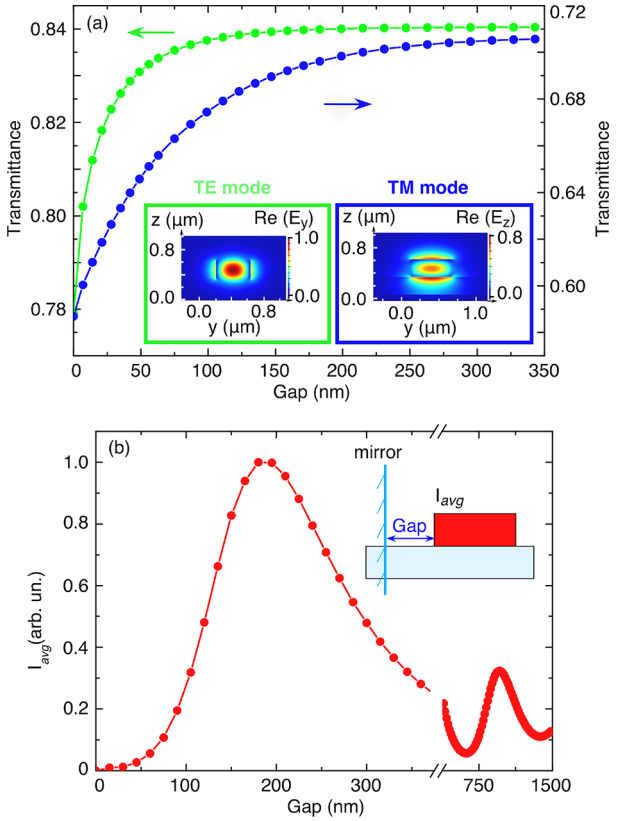

Figure 4. (a) Waveguide transmittance for two fundamental modes (TE and TM) as a function of the gap between the nanodisk and the waveguide; insets show the profiles of TE and TM mode, correspondingly. (b) Normalized local electric fields, given by eq 1, as a function of the gap between the nanodisk and the mirror; inset illustrates the sketch of numerical simulation.

comparing the FWHM dependence on L to that of the average local fields $I_{\mathrm{avg}}(L)$, given by the dashed red curve, one can conclude that the main contribution to the alternating local fields of the nanodisk is provided by the dependence of the MD resonance radiative decay constant. We can, therefore, infer that the nonmonotonic dependence of the measured TH signal as a function of the gap size represents an observation of optical coupling between the nanodisk and the nanowire that modifies both the central frequency and the lifetime of the MD mode.

The nanowires under study support propagation of two fundamental modes (TE and TM) with electric field vector parallel and perpendicular to the substrate, correspondingly (see insets in Figure 4a). The presence of a nanodisk with a diameter of 480 nm influences the waveguide modes, as shown in Figure 4a. When the nanodisk is close to the waveguide, the TE mode transmittance decreases from 0.84 at the gap $L \approx$ 80 nm to 0.78 at the gap L = 0 nm. At the same time, the TM mode transmittance decreases from 0.71 at the gap $L \approx$ 300 nm to 0.59 at the gap L = 0 nm. It can be concluded that the TM mode is influenced stronger by the nanodisk. This happens because of the configuration of electric field outside the nanodisk at the MD resonance that matches the direction of electric field of the TM mode. Naturally, the nanodisk with a diameter of 480 nm has a stronger influence on the TM mode than the nanodisks with smaller diameters of 430 and 380 nm. The dependence of the TM mode transmittance on the gap and the nanodisk diameter is provided in Supporting

DOI: 10.1021/acsphotonics.8b01386
ACS Photonics 2019, 6, 189−195

Information. Thus, we can infer that the regime of optical coupling between the nanodisk's MD-resonance and the waveguide's TM mode can be realized at the gap sizes less than about 200 nm. We believe it is the presence of the coupling channel between the far-field scattering and the TM mode influences the overall level of the THG signal observed at these gap sizes. As the next step, an intriguing continuation of the present research would be to directly couple light from within the waveguide to isolated resonant silicon nanodisk or silicon-based metasurfaces.

To conclude, we have performed nonlinear microscopy of resonant all-dielectric nanoparticles optically coupled to dielectric nanowires that support fundamental waveguiding modes at the pump frequency. Third harmonic generation from subwavelength silicon nanodisks is enhanced by a factor of 25 with respect to bulk silicon when its fundamental magnetic dipolar mode is resonantly excited by femtosecond laser pulses at λ = 1.545 μm. The third harmonic signal is shown to significantly depend on the distance between the nanodisk and the nanowire, with the maximum detected modulation of up to 4.5. The presence of the nanowire was found to increase the third harmonic output from the nanodisk, which is explained by a redistribution of the local fields and reduction of radiative losses of the system, that results in a higher average third-order nonlinear polarization. At the same time, when the nanodisk is closer than 200 nm to the nanowire, the MD-resonance of nanodisk is coupled to TM mode of waveguide, as revealed by full-wave simulations of the waveguide transmittance. We render these results an important step toward the integration of resonant all-dielectric nanostructures on photonic chips.

METHODS

THG and Confocal Microscopy. For THG and confocal laser scanning microscopy (CLSM), we used an Olympus FluoView FV1000 laser scanning confocal microscope in combination with a femtosecond Er^{3+} fiber laser equipped with amplifier (Avesta EFOA-100) with 150 fs-long pulses with a carrier wavelength of λ = 1.545 μm and a repetition rate of 70 MHz. CLSM was configured on an Olympus IX81 automated inverted microscope platform with an XY automated stage Prior H117N2IX and equipped with spectral (variable bandpass) detector, filter-based detectors and a laser combiner that allowed multiwavelength operation. A 635 nm CW laser was used for CLSM image formation in reflection. As a result, THG and reflection CLSM images were captured simultaneously as detected by two separate photomultipliers (PMT) at wavelengths from 515 to 535 nm (results from Table 1) or from 512 to 518 nm (results from Figure 3) and 635 nm, respectively. Detected signals were separated by an edge filter SDM560, a bandpass filter BA575−675 and a monochromator in front of one of the PMTs. Additionally, this approach allowed one to avoid two-photon absorption of the pump radiation at the PMT cathode. In THG microscopy measurements, a femtosecond laser beam passed through a polarizer (Glan prism) and focused at the sample into a spot with a diameter of 3 μm by an aspheric lens ThorLabs C610TME-B with NA = 0.6 and a focal length of 4 mm. The polarizer orientation was chosen to be either perpendicular or parallel to the nanowires. Both these polarizations were directed at an angle of ±45° relative to the polarization of the original laser radiation. The position of the sample relative to the waist of the pump radiation was adjusted by the XY automated stage of CLSM. The transmission radiation and THG were both collected by an UPLSAPO 40× objective with NA = 0.9.

Calculations. For numerical calculations of the THG and the local field distribution, we used the commercial software package Lumerical FDTD Solutions, in which the simulation area was constrained by perfectly matched layer boundary conditions. A normally impinging broadband Gaussian beam was chosen as a light source. It was located in the SiO_2 substrate and focused into a waist of about 3 μm in diameter and divergence angle of ≈5°. The dimensions of the structure were as follows: the SiO_2 layer was 277 nm in thickness, the silicon nanowire was 280 nm in height and 445 nm in width, and the nanodisks were 280 nm in height and 380, 430, or 480 nm in diameter. The gaps between silicon nanowire and silicon nanodisks were 90, 185, or 315 nm.

Sample Fabrication and Characterization. The samples of the "silicon nanodisk−nanowire" pairs were fabricated out of the SOI (silicon-on-insulator wafers) with thicknesses of both the device silicon and the buried SiO_2 layers of 280 nm, and a silicon 400 μm thick substrate. The wafers were cleaned with organic solvents in an ultrasonic bath. The mask was exposed by e-beam lithography tool Raith150 at 30 kV. The resist was HSQ with a thickness of 180 nm. A standard developer 25% TMAH solution in water was used. Silicon was etched in Oxford PlasmaPro by a fluorine plasma process. The residue of mask after the etching was removed in a low-concentrated solution of HF.

The width of silicon nanowire, the diameters of silicon nanodisks and the gaps between them were determined by scanning electron microscopy (Zeiss Supra 40). Calculations of nanowire's and nanodisk's dimensions was performed using SmartSEM software.

The thickness of SiO_2 layer was determined by spectroscopic ellipsometry which was carried out with a phase modulated spectroscopic ellipsometer Horiba Jobin-Yvon UVISEL 2. The data were acquired over photon energy from 1.5 to 6 eV at two different angles of incidence (50° and 70°) and at two different regions of the sample. Calculation of SiO_2 thickness was done by Horiba Jobin-Yvon DeltaPsi 2 software. Optical properties of Si substrate[38] and SiO_2 layer[39] were used for the thickness calculation.

The thickness of nanowires and disks was determined by atomic force microscopy (AFM). Results were obtained using a scanning probe microscope NT-MDT NTEGRA Prima. Silicon AFM probes NT-MDT NSG10 series were employed. The measurements were performed in the semicontact mode. Amplitude (peak-to-peak) of the "free-air" probe oscillations was from 45 to 30 nm.

ASSOCIATED CONTENT

Supporting Information

The Supporting Information is available free of charge on the ACS Publications website at DOI: 10.1021/acsphotonics.8b01386.

Blue-shifted MD mode for smaller nanodisk diameters; Experimental THG enhancement data for the orthogonal pump polarization; Local electric fields within the nanodisks with different diameters; Waveguide TM mode transmittance depending on the gap size and nanodisk diameter (PDF).

DOI: 10.1021/acsphotonics.8b01386
ACS Photonics 2019, 6, 189−195

AUTHOR INFORMATION

Corresponding Author

*E-mail: fedyanin@nanolab.phys.msu.ru.

ORCID

Alexander A. Ezhov: 0000-0001-6221-3093

Andrey A. Fedyanin: 0000-0003-4708-6895

Notes

The authors declare no competing financial interest.

ACKNOWLEDGMENTS

The authors thank I. V. Bozhev for scanning electron microscopy. We thank Y. S. Kivshar, B. S. Lukyanchuk, and A. A. Popkova for insightful discussions. This work was partly supported by Russian Ministry of Education and Science (#14.W03.31.0008, calculation of local fields) and MSU Quantum Technology Center. THG experiments were performed with the support of Russian Foundation for Basic Research (#16-02-01092 and #18-32-01073). Nonlinear FDTD calculations were supported by Russian Science Foundation (#18-12-00475).

REFERENCES

(1) Atwater, H. A.; Polman, A. Plasmonics for improved photovoltaic devices. *Nat. Mater.* **2010**, *9*, 205−213.

(2) Jain, P. K.; Huang, X.; El-Sayed, I. H.; El-Sayed, M. A. Noble metals on the nanoscale: optical and photothermal properties and some applications in imaging, sensing, biology, and medicine. *Acc. Chem. Res.* **2008**, *41*, 1578−1586.

(3) Jain, P. K.; Lee, K. S.; El-Sayed, I. H.; El-Sayed, M. A. Calculated absorption and scattering properties of gold nanoparticles of different size, shape, and composition: applications in biological imaging and biomedicine. *J. Phys. Chem. B* **2006**, *110*, 7238−7248.

(4) Kelly, K. L.; Coronado, E.; Zhao, L. L.; Schatz, G. C. The optical properties of metal nanoparticles: the influence of size, shape, and dielectric environment. *J. Phys. Chem. B* **2003**, *107*, 668−677.

(5) Rechberger, W.; Hohenau, A.; Leitner, A.; Krenn, J.; Lamprecht, B.; Aussenegg, F. Optical properties of two interacting gold nanoparticles. *Opt. Commun.* **2003**, *220*, 137−141.

(6) Halas, N. J.; Lal, S.; Chang, W. S.; Link, S.; Nordlander, P. Plasmons in strongly coupled metallic nanostructures. *Chem. Rev.* **2011**, *111*, 3913−3961.

(7) Liu, N.; Hentschel, M.; Weiss, T.; Alivisatos, A. P.; Giessen, H. Three-dimensional plasmon rulers. *Science* **2011**, *332*, 1407−1410.

(8) Maier, S. A.; Kik, P. G.; Atwater, H. A.; Meltzer, S.; Harel, E.; Koel, B. E.; Requicha, A. A. Local detection of electromagnetic energy transport below the diffraction limit in metal nanoparticle plasmon waveguides. *Nat. Mater.* **2003**, *2*, 229−232.

(9) Jain, P. K.; Huang, W.; El-Sayed, M. A. On the universal scaling behavior of the distance decay of plasmon coupling in metal nanoparticle pairs: a plasmon ruler equation. *Nano Lett.* **2007**, *7*, 2080−2088.

(10) Teperik, T. V.; Nordlander, P.; Aizpurua, J.; Borisov, A. G. Robust subnanometric plasmon ruler by rescaling of the nonlocal optical response. *Phys. Rev. Lett.* **2013**, *110*, 263901.

(11) Shcherbakov, M. R.; Le, A. T.; Dubrovina, N.; Lupu, A.; Fedyanin, A. A. Plasmon ruler with gold nanorod dimers: utilizing the second-order resonance. *Opt. Lett.* **2015**, *40*, 1571−1574.

(12) Evlyukhin, A. B.; Reinhardt, C.; Seidel, A.; Lukyanchuk, B. S.; Chichkov, B. N. Optical response features of Si-nanoparticle arrays. *Phys. Rev. B: Condens. Matter Mater. Phys.* **2010**, *82*, No. 045404.

(13) Kuznetsov, A. I.; Miroshnichenko, A. E.; Brongersma, M. L.; Kivshar, Y. S.; Lukyanchuk, B. S. Optically resonant dielectric nanostructures. *Science* **2016**, *354*, aag2472.

(14) Kruk, S. S.; Kivshar, Y. S. Functional meta-optics and nanophotonics governed by Mie resonances. *ACS Photonics* **2017**, *4*, 2638−2649.

(15) Kuznetsov, A. I.; Miroshnichenko, A. E.; Fu, Y. H.; Zhang, J.; Lukyanchuk, B. S. Magnetic light. *Sci. Rep.* **2012**, *2*, 492.

(16) Evlyukhin, A. B.; Novikov, S. M.; Zywietz, U.; Eriksen, R. L.; Reinhardt, C.; Bozhevolnyi, S. I.; Chichkov, B. N. Demonstration of magnetic dipole resonances of dielectric nanospheres in the visible region. *Nano Lett.* **2012**, *12*, 3749−3755.

(17) Bakker, R. M.; Permyakov, D.; Yu, Y. F.; Markovich, D.; Paniagua-Domnguez, R.; Gonzaga, L.; Samusev, A.; Kivshar, Y. S.; Lukyanchuk, B. S.; Kuznetsov, A. I. Magnetic and electric hotspots with silicon nanodimers. *Nano Lett.* **2015**, *15*, 2137−2142.

(18) Wang, L.; Kruk, S.; Xu, L.; Rahmani, M.; Smirnova, D.; Solntsev, A.; Kravchenko, I.; Neshev, D.; Kivshar, Y. Shaping the third-harmonic radiation from silicon nanodimers. *Nanoscale* **2017**, *9* (6), 2201−2206.

(19) Shcherbakov, M. R.; Shorokhov, A. S.; Neshev, D. N.; Hopkins, B.; Staude, I.; Melik-Gaykazyan, E. V.; Ezhov, A. A.; Miroshnichenko, A. E.; Brener, I.; Fedyanin, A. A.; Kivshar, Y. S. Nonlinear interference and tailorable third-harmonic generation from dielectric oligomers. *ACS Photonics* **2015**, *2*, 578−582.

(20) Hopkins, B.; Poddubny, A. N.; Miroshnichenko, A. E.; Kivshar, Y. S. Revisiting the physics of Fano resonances for nanoparticle oligomers. *Phys. Rev. A: At., Mol., Opt. Phys.* **2013**, *88*, No. 053819.

(21) Shorokhov, A. S.; Melik-Gaykazyan, E. V.; Smirnova, D. A.; Hopkins, B.; Chong, K. E.; Choi, D.-Y.; Shcherbakov, M. R.; Miroshnichenko, A. E.; Neshev, D. N.; Fedyanin, A. A.; Kivshar, Y. S. Multifold enhancement of third-harmonic generation in dielectric nanoparticles driven by magnetic Fano resonances. *Nano Lett.* **2016**, *16*, 4857−4861.

(22) Shcherbakov, M. R.; Neshev, D. N.; Hopkins, B.; Shorokhov, A. S.; Staude, I.; Melik-Gaykazyan, E. V.; Decker, M.; Ezhov, A. A.; Miroshnichenko, A. E.; Brener, I.; Fedyanin, A. A.; Kivshar, Y. S. Enhanced third-harmonic generation in silicon nanoparticles driven by magnetic response. *Nano Lett.* **2014**, *14*, 6488−6492.

(23) Yang, Y.; Wang, W.; Boulesbaa, A.; Kravchenko, I. I.; Briggs, D. P.; Puretzky, A.; Geohegan, D.; Valentine, J. Nonlinear Fano-resonant dielectric metasurfaces. *Nano Lett.* **2015**, *15*, 7388−7393.

(24) Liu, S.; Sinclair, M. B.; Saravi, S.; Keeler, G. A.; Yang, Y.; Reno, J.; Peake, G. M.; Setzpfandt, F.; Staude, I.; Pertsch, T.; Brener, I. Resonantly enhanced second-harmonic generation using III−V semiconductor all-dielectric metasurfaces. *Nano Lett.* **2016**, *16*, 5426−5432.

(25) Shcherbakov, M. R.; Liu, S.; Zubyuk, V. V.; Vaskin, A.; Vabishchevich, P. P.; Keeler, G.; Pertsch, T.; Dolgova, T. V.; Staude, I.; Brener, I.; Fedyanin, A. A. Ultrafast all-optical tuning of direct-gap semiconductor metasurfaces. *Nat. Commun.* **2017**, *8*, 17.

(26) Melik-Gaykazyan, E. V.; Kruk, S. S.; Camacho-Morales, R.; Xu, L.; Rahmani, M.; Zangeneh Kamali, K.; Lamprianidis, A.; Miroshnichenko, A. E.; Fedyanin, A. A.; Neshev, D. N.; Kivshar, Y. S. Selective third-harmonic generation by structured light in Mie-resonant nanoparticles. *ACS Photonics* **2018**, *5*, 728−733.

(27) Wang, L.; Kruk, S. S.; Koshelev, K. L.; Kravchenko, I. I.; Luther-Davies, B.; Kivshar, Y. S. Nonlinear wavefront control with all-dielectric metasurfaces. *Nano Lett.* **2018**, *18*, 3978−3984.

(28) Staude, I.; Schilling, J. Metamaterial-inspired silicon nanophotonics. *Nat. Photonics* **2017**, *11*, 274−284.

(29) Bakker, R. M.; Yu, Y. F.; Paniagua-Domnguez, R.; Lukyanchuk, B. S.; Kuznetsov, A. I. Resonant light guiding along a chain of silicon nanoparticles. *Nano Lett.* **2017**, *17*, 3458−3464.

(30) Cheben, P.; Halir, R.; Schmid, J. H.; Atwater, H. A.; Smith, D. R. Subwavelength integrated photonics. *Nature* **2018**, *560* (7720), 565.

(31) Frolov, A. Y.; Verellen, N.; Li, J.; Zheng, X.; Paddubrouskaya, H.; Denkova, D.; Shcherbakov, M. R.; Vandenbosch, G. A.; Panov, V. I.; Van Dorpe, P.; Fedyanin, A. A.; Moshchalkov, V. V. Near-Field Mapping of Optical Fabry−Perot Modes in All-Dielectric Nanoantennas. *Nano Lett.* **2017**, *17*, 7629−7637.

(32) Gongora, J. S. T.; Miroshnichenko, A. E.; Kivshar, Y. S.; Fratalocchi, A. Anapole nanolasers for mode-locking and ultrafast pulse generation. *Nat. Commun.* **2017**, *8*, 15535.

DOI: 10.1021/acsphotonics.8b01386
ACS Photonics 2019, 6, 189−195

(33) Rodrguez-Fortuño, F. J.; Barber-Sanz, I.; Puerto, D.; Griol, A.; Martnez, A. Resolving light handedness with an on-chip silicon microdisk. *ACS Photonics* **2014**, *1*, 762−767.
(34) Espinosa-Soria, A.; Rodrguez-Fortuño, F. J.; Griol, A.; Martnez, A. On-Chip optimal stokes nanopolarimetry based on spin−orbit interaction of light. *Nano Lett.* **2017**, *17*, 3139−3144.
(35) Staude, I.; Miroshnichenko, A. E.; Decker, M.; Fofang, N. T.; Liu, S.; Gonzales, E.; Dominguez, J.; Luk, T. S.; Neshev, D. N.; Brener, I.; Kivshar, Y. S. Tailoring directional scattering through magnetic and electric resonances in subwavelength silicon nanodisks. *ACS Nano* **2013**, *7*, 7824−7832.
(36) Hon, N. K.; Soref, R.; Jalali, B. The third-order nonlinear optical coefficients of Si, Ge, and Si_{1-x} Ge_x in the midwave and longwave infrared. *J. Appl. Phys.* **2011**, *110*, 011301.
(37) Gubler, U.; Bosshard, C. Optical third-harmonic generation of fused silica in gas atmosphere: Absolute value of the third-order nonlinear optical susceptibility $\chi^{(3)}$. *Phys. Rev. B: Condens. Matter Mater. Phys.* **2000**, *61*, 10702.
(38) Jellison, G. E. Optical functions of silicon determined by two-channel polarization modulation ellipsometry. *Opt. Mater.* **1992**, *1*, 41−47.
(39) Palik, E. D. Handbook of optical constants of solids. *Handbook of Optical Constants of Solids*; Elsevier, 1985; Vol. *1*, p 749.

DOI: 10.1021/acsphotonics.8b01386
ACS Photonics 2019, 6, 189−195